
Kinetics of Perrhenate Uptake and Comparative Biodistribution of Perrhenate, Pertechnetate, and Iodide by NaI Symporter–Expressing Tissues In Vivo

Lionel S. Zuckier, MD¹; Orshi Dohan, MD²; Yi Li, MD³; Chee Jen Chang, PhD⁴; Nancy Carrasco, MD²; and Ekaterina Dadachova, PhD³

¹Department of Radiology, New Jersey Medical School, Newark, New Jersey; ²Department of Molecular Pharmacology, Albert Einstein College of Medicine, Bronx, New York; ³Department of Nuclear Medicine, Albert Einstein College of Medicine, Bronx, New York; and ⁴Department of Medical Research, National Taiwan University Hospital, Taipei, Taiwan

Pertechnetate (as $^{99m}\text{TcO}_4^-$, $^{123}\text{I}^-$, and $^{131}\text{I}^-$) have a long and successful history of use in the diagnosis and therapy of thyroid cancer, with uptake into thyroid tissue mediated by the sodium-iodide symporter (NIS). NIS has also emerged as a potential target for radiotherapy of nonthyroid malignancies that express the endogenous or transfected symporter. Perrhenates (as $^{188}\text{ReO}_4^-$ and $^{186}\text{ReO}_4^-$) are promising therapeutic substrates of NIS, although less is known about their behavior in vivo. In this study, we endeavored to characterize the biologic behavior of perrhenate, especially in relation to iodide and pertechnetate, to better explore its possible therapeutic role. **Methods:** We describe the simultaneous biodistribution and uptake in vivo of iodide, pertechnetate, and perrhenate in groups of healthy CD1 mice, either with or without coadministration of perchlorate (ClO_4^-), a potent NIS inhibitor. Animals administered single radiopharmaceuticals were imaged as a means of illustrating these findings. Kinetic properties of perrhenate were compared with those of iodide in a stably transfected NIS-bearing Madin-Darby canine kidney (MDCK) cell line. **Results:** Biodistributions of iodide, pertechnetate, and perrhenate in live mice were remarkably similar. Activity in salivary gland and stomach was severalfold greater than in blood, remained elevated over the initial 2 h, and subsequently washed out. A similar pattern characterized pertechnetate and perrhenate uptake by the thyroid, in which the 2-h concentration was slightly more elevated than at the 20-min time point. However, uptake subsequently decreased by 19 h. In contrast, iodide continued to increase through the 19-h time point, presumably as a result of organification. The addition of perchlorate sharply decreased uptake of all 3 radiopharmaceuticals by the stomach, salivary glands, and thyroid and resulted in their rapid clearance, paralleling blood-pool clearance. In tissues that do not express NIS (liver, muscle, spleen), uptake of all 3 radiopharmaceuticals was low and rapidly decreased over time, paralleling blood-pool clearance. Similar findings were seen in kidney, where only minimal

amounts of NIS are expressed in tubular cells. In stably transfected MDCK cells, steady-state accumulation of iodide was approximately 4-fold higher than that of perrhenate at 30 min. No active transport was demonstrated in nontransfected MDCK cell lines or after perchlorate administration. Uptake values measured at different concentrations of substrate demonstrated saturation kinetics. Apparent maximal velocity values for perrhenate and iodide were 25.6 ± 1.4 and 106 ± 3.2 pmol/ μg , respectively, and corresponding affinity constant values were 4.06 ± 0.87 and 24.6 ± 1.81 $\mu\text{mol/L}$. **Conclusion:** Perrhenate is avidly taken up by NIS in a manner similar to iodide and pertechnetate in vivo, with the exception of organification of iodide by the thyroid. By more fully appreciating the behavior of perrhenate, especially in relation to iodide and pertechnetate, we can better realize its potential role in the diagnosis and therapy of NIS-bearing tissues.

Key Words: dosimetry; oncology; radiobiology; radionuclide therapy; perrhenate; pertechnetate; radiotherapy; sodium-iodide symporter

J Nucl Med 2004; 45:500–507

Iodide, in the form of $^{123}\text{I-NaI}$ and $^{131}\text{I-NaI}$, has been used extensively in the imaging and treatment of hyperthyroidism and thyroid carcinoma. Uptake of iodide into thyroid tissue is mediated by the sodium-iodide symporter (NIS). Since cloning of the rat (1) and the human (2) forms of the molecule in 1996, NIS has been the subject of numerous studies concerning structure and function relationships and regulation (3–8). NIS-mediated active transport of iodide is driven by the Na^+ electrochemical gradient generated by Na^+/K^+ -adenosine triphosphatase, with 2 Na^+ ions translocated into the cells per each iodide ion (9). NIS also mediates iodide uptake into other tissues known to concentrate iodide, such as stomach, salivary gland, and lactating breast (4). NIS expression has also been demonstrated in more than 80% of human mammary cancers, raising the possibility of administering $^{131}\text{I-NaI}$ for therapy of breast malignancies.

Received Aug. 14, 2003; revision accepted Nov. 3, 2003.

For correspondence or reprints contact: Lionel S. Zuckier, MD, Department of Radiology, New Jersey Medical School, P.O. Box 1709, Newark, NJ 07101-1709.

E-mail: zuckier@umdnj.edu

nancy (10–12). Furthermore, considerable interest has been expressed regarding radioiodide therapy after targeted transfection of NIS-containing vectors into non-NIS-bearing malignant tissues (13–16).

Although its main physiologic role is transport of iodide, NIS has been shown to transport other structurally similar anions. For example, pertechnetate (TcO_4^-) shares physicochemical attributes with iodide and exhibits similar biodistribution on radionuclide scanning, with the exception of organification within the thyroid, which occurs only with iodide. $^{99\text{m}}\text{TcO}_4^-$ has therefore achieved an important clinical role as a surrogate for iodide in radionuclide imaging of NIS-dependent functions, including transport of substrate into the thyroid gland (historically known as “trapping”) and secretory function of the salivary glands and gastric mucosa (17–19). More recently, another structurally similar anion, perrhenate (ReO_4^-), has been proposed as a therapeutic radiopharmaceutical for treatment of NIS-bearing tumors (20). Rhenium, like technetium, is a member of the group VIIA elements of the periodic table. The radioactive moiety $^{188}\text{ReO}_4^-$ is easily eluted from a $^{188}\text{W}/^{188}\text{Re}$ generator system. ^{188}Re has a half-life of 17 h and emits high-energy β^- particles ($E_{\text{av}} = 0.795$ MeV) and an imageable 155-keV γ -photon. Alternatively, perrhenate may be produced incorporating the reactor product ^{186}Re . This radionuclide has a half-life of 91 h and emits medium-range β^- particles ($E_{\text{av}} = 0.362$ MeV) and an imageable 137-keV γ -photon.

The biodistribution and properties of iodide and pertechnetate have been relatively well characterized, whereas less is known about perrhenate (20–23). As a close analog of pertechnetate, perrhenate would be expected to exhibit similar physical properties and binding behavior (24). Nonetheless, significant differences in chemical properties, such as reduction potential, may quantitatively alter the behavior of perrhenate *in vivo* (24). Fewer similarities are expected between perrhenate and iodide.

We have endeavored to characterize the biologic behavior of perrhenate using 2 techniques. We describe the simultaneous biodistribution of iodide, pertechnetate, and perrhenate in healthy CD1 mice to compare and contrast biodistribution and uptake *in vivo*. Additional mice administered single radiopharmaceuticals were imaged to illustrate these findings. These biodistribution studies were, to some degree, qualitative, in that the amount of substrate could not be readily controlled in a living animal in contrast to cell culture assays, in which the amounts of substrate can be rigorously controlled. We therefore also permanently transfected the Madin–Darby canine kidney (MDCK) cell line with NIS to characterize the kinetic properties of perrhenate uptake and compare them with those of iodide (7). By more fully understanding the behavior of perrhenate, especially in relation to iodide and pertechnetate, we begin to explore its possible role in diagnosis and therapy of NIS-bearing tissues, an area of emerging clinical interest (25).

MATERIALS AND METHODS

In Vivo Biodistribution

$^{99\text{m}}\text{TcO}_4^-$ (630 KBq), $^{188}\text{ReO}_4^-$ (630 KBq), and $^{125}\text{I}^-$ (63 KBq) in 0.1 mL of phosphate-buffered saline (PBS) were coinjected in the tail vein in mice, with or without the addition of 2 mg of perchlorate (ClO_4^-), a powerful NIS blocker. Fifteen animals were in each group. $^{99\text{m}}\text{TcO}_4^-$ was obtained commercially from a freshly eluted $^{99}\text{Mo}/^{99\text{m}}\text{Tc}$ generator (Syncor International). $^{188}\text{ReO}_4^-$ was locally eluted from a $^{188}\text{W}/^{188}\text{Re}$ generator (Oak Ridge National Laboratory). $^{125}\text{I}^-$ was obtained commercially (NEN). Within each group, 5 mice were killed at each of 20 min, 2 h, and 19 h. Eight tissues of interest (liver, muscle, spleen, kidney, blood, salivary gland, thyroid, and stomach) were removed and weighed on an analytic balance. $^{99\text{m}}\text{Tc}$ and ^{188}Re were counted immediately using asymmetric windows and a dual-isotope-correcting program (Compu-gamma 1282; LKB Wallac); ^{125}I was counted 8 d thereafter, after $^{99\text{m}}\text{Tc}$ and ^{188}Re decay. Uptake was expressed as percentage of injected dose per gram of tissue (%ID/g) by comparison to a reference standard of injectate. For each radiopharmaceutical, a localization ratio was also generated by expressing the ratio of %ID/g in each tissue to that in blood.

To further illustrate the distribution of radionuclide visually, single anesthetized animals were injected with 18 MBq of $^{123}\text{I}^-$, $^{99\text{m}}\text{TcO}_4^-$, or $^{188}\text{ReO}_4^-$ and imaged supine on a dedicated research γ -camera (Picker Dynacamera 4C; Picker International) and computer system (Nuclear MAC; Scientific Imaging, Inc.) using a pinhole collimator positioned 13 cm above the animals. Images with 20% windows centered on each photopeak were dynamically acquired for 20 min after injection and thereafter at 24 min, 60 min, and 24 h. Standard-sized regions of interest (ROIs) were drawn around the thyroid, mediastinum, and stomach to derive time–activity curves that were normalized according to the total count rate of the initial images. Counts in each ROI were expressed in percentage of injected dose per ROI (%ID/ROI).

Generation of MDCK Cells Permanently Transfected with NIS

MDCK cells were transfected with the pcDNA 3.1(–) plasmid containing the human NIS cDNA, by means of the Eugene 6 transfection reagent (Roche), according to the manufacturer’s instructions. After selection in media containing 1 mg/mL Geneticin (G418 sulfate; GIBCO-BRL), NIS-expressing clones were isolated and expanded. The clone with the highest iodide uptake was used for these experiments.

Transport in Cultured Cells

Uptake of perrhenate and iodide using stably hNIS-transfected MDCK cells was characterized both as a function of time and of substrate concentration, according to previously described methods (1,7,26). Transport assays were determined in triplicate. For uptake experiments, cells grown in 12-well plates were washed twice with 1 mL of HEPES-buffered Hanks’ balanced salt solution (buffered HBSS) and incubated with buffered HBSS containing 20 $\mu\text{mol/L}$ perrhenate or NaI supplemented with carrier-free $^{188}\text{ReO}_4^-$ or Na^{125}I , to give specific activities of 3.7 GBq/mmol. Additional control experiments were performed in the presence of the NIS inhibitor perchlorate (40 $\mu\text{mol/L}$) or using nontransfected MDCK cells. Incubations proceeded at 37°C for given reaction times in a humidified

atmosphere and were terminated by aspirating the radioactive medium and washing twice with 1 mL ice-cold HBSS. Cells were made permeable with 500 μ L of 95% ethanol (4°C) for 20 min and counted in a γ -counter. The DNA content of each well was subsequently determined after trichloroacetic acid precipitation, by the diphenylamine method (27). Based on the specific activity of the substrates, the efficiency of the γ -counter, and the DNA content of each well, iodide and perrhenate uptake were expressed as picomoles of substrate transported per microgram of DNA.

The time courses of uptake of perrhenate and iodide were determined after incubation of substrate at concentrations of 20 μ mol/L for 5, 10, and 30 min in both hNIS-transfected and nontransfected MDCK cells. Additional measurements at 30 min were performed in the presence of perchlorate.

The effect of substrate concentration on uptake was determined by incubating washed cells for 2 min in medium containing 8 concentrations of either perrhenate or iodide, ranging between 0.625 and 80 μ mol/L. Uptake reactions were then terminated and substrate uptake was quantitated as indicated above. Data were fitted to the theoretic model ($v = V_{max} \times [\text{anion}] / K_m + [\text{anion}]$), where V_{max} is maximal velocity and K_m is the affinity constant, by nonlinear least squares using the Marquard-Levenberg algorithm to yield V_{max} and K_m values (7,28).

RESULTS

The biodistributions of iodide, pertechnetate, and perrhenate in live mice were remarkably similar. Activity in blood (Fig. 1) decreased stepwise over time, with little activity remaining at 19 h. Activity in NIS-expressing salivary gland was severalfold greater than in blood, remained elevated over the initial 2 h, and subsequently washed out (Fig. 1). In the stomach, the concentration of activity was even higher than that in salivary gland at 20 min and continued to increase through 2 h, thereafter falling by the 19-h time point. Similar patterns characterized pertechnetate and perrhenate uptake by the thyroid, in which the 2-h concentration was slightly more elevated than the 20-min time point. However, uptake subsequently decreased by 19 h. In contrast, iodide continued to increase through the 19-h time point, presumably as a result of organification (Fig. 1). Coinjection of perchlorate resulted in a relative increase in vascular activity at 20 min, probably because it was not removed by NIS-bearing organs when this potent NIS-inhibitor was administered. Addition of perchlorate sharply decreased uptake of all 3 radiopharmaceuticals by the stom-

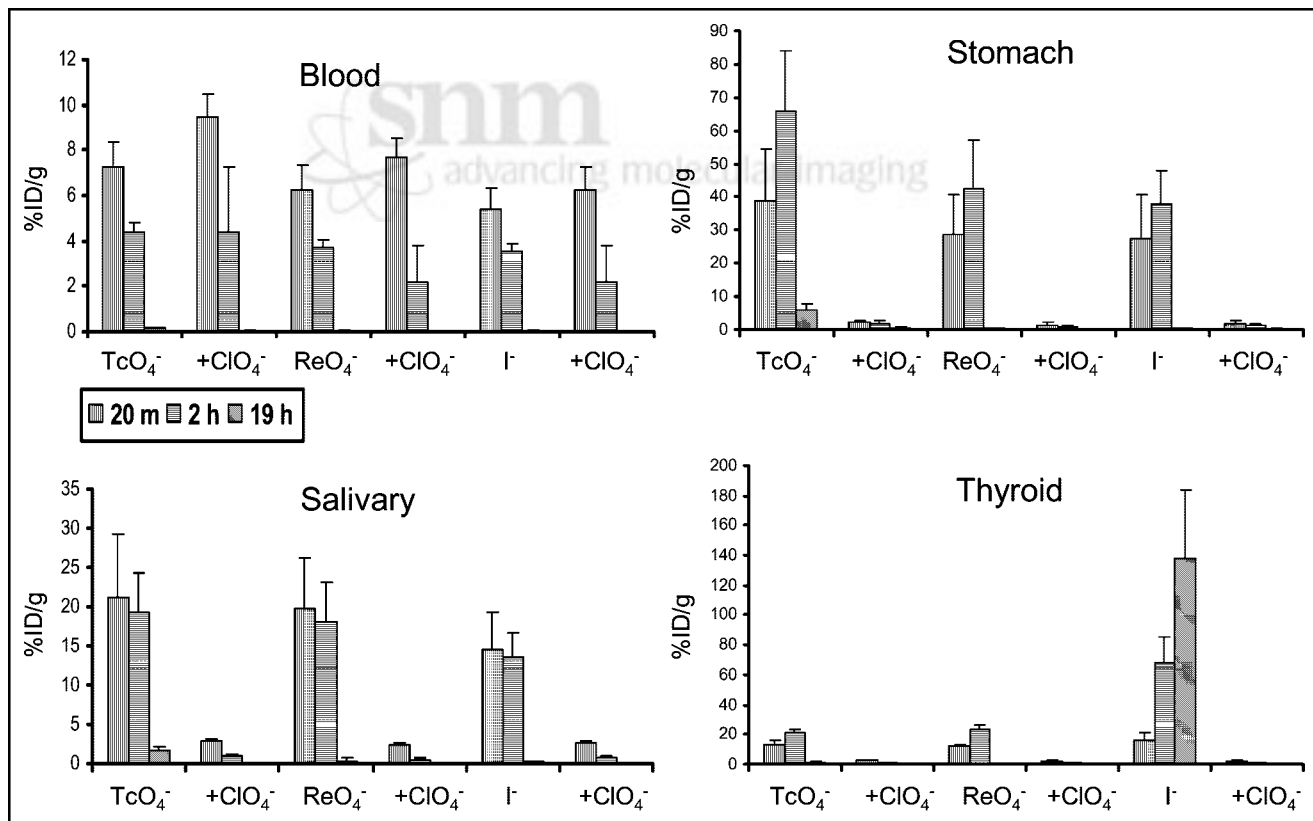


FIGURE 1. Activity in blood and NIS-expressing tissues. Error bars represent 1 SD. Note the variable y-axis scales. Radiopharmaceutical uptake was similar for the 3 radiopharmaceutical substrates, with the exception of iodide in the thyroid. Blood activity gradually decreased with time and was noted to be slightly greater in mice administered perchlorate, as a result of absence of competing excretory pathways. Uptake in NIS-expressing stomach and salivary gland was relatively high, remained elevated or increased over the initial 2 h, and subsequently washed out. This pattern also characterized perrhenate and pertechnetate uptake in the thyroid. However, iodide continued to increase through the 19-h time point, presumably as a result of organification. Blocking of NIS by coinjection of perchlorate decreased uptake of all 3 radiopharmaceuticals by the stomach, salivary glands, and thyroid and resulted in their rapid clearance, paralleling clearance in blood.

ach, salivary glands, and thyroid and resulted in their rapid clearance, paralleling clearance from the blood pool (Fig. 1).

Activity in tissues that do not express NIS (liver, muscle, spleen) was low and rapidly decreased over time (Fig. 2), paralleling blood-pool clearance (Fig. 1). Although some studies have reported small amount of NIS expression in cells in the collecting tubule of the kidney, the pattern of uptake we observed in the kidneys resembled that of tissues without significant NIS expression (Fig. 2) (29). Addition of perchlorate did not greatly change the magnitude of uptake in these tissues, although there was a tendency for the activity to be slightly higher at 20 min in the kidney, probably as a result of the absence of competition by NIS-bearing organs. Uptake by various tissues at 20 min and 2 h was also expressed as a localization ratio of the specific activity in each tissue to that of the blood (Table 1). Uptake ratios for each of the 3 radiopharmaceuticals in thyroid, stomach, and salivary glands were >1 and increased between the 20-min and 2-h time points. Liver, spleen, kidney, and muscle, as well as all organs in the presence of perchlorate, had ratios <1 .

Images in representative mice (Fig. 3) demonstrated the marked amount of gastric uptake noted for all 3 radiopharmaceuticals on the 24- and 60-min images. By 24 h, the stomach was less well defined and, at least in the case of

$^{99m}\text{TcO}_4^-$, activity appeared to be more distally located within the bowel. For $^{99m}\text{TcO}_4^-$ and $^{188}\text{ReO}_4^-$, a modest amount of concentration of activity was seen in the region of the thyroid gland at 24 and 60 min, but this faded by the 24-h time point. In contrast, $^{123}\text{I}^-$ gradually increased between the 24-min, 60-min, and 24-h images. Time-activity curves based on ROIs over the stomach, mediastinum, and thyroid (Fig. 3) demonstrated similar appearances for the 3 radiopharmaceuticals over 60 min. Uptake in the stomach was most intense and increased over the 1 h of initial imaging, reaching 20%–25% of injected activity. The magnitude of thyroid uptake was less, reaching 5%–7% of injected activity. In contrast, mediastinal activity, reflecting blood pool, gradually decreased over the initial 1 h of measurement, constituting approximately 2% of injected activity at the 60-min time point.

To formally assess the transport properties of perrhenate accumulation by NIS, we investigated the time course of accumulation of both iodide and perrhenate in hNIS-transfected MDCK cells (Fig. 4A). Steady-state uptake was approximately 4-fold higher for iodide than for perrhenate at the 30-min time point. No active transport was demonstrated in the nontransfected MDCK cell lines, whereas the addition of perchlorate effectively blocked uptake in the transfected cell line.

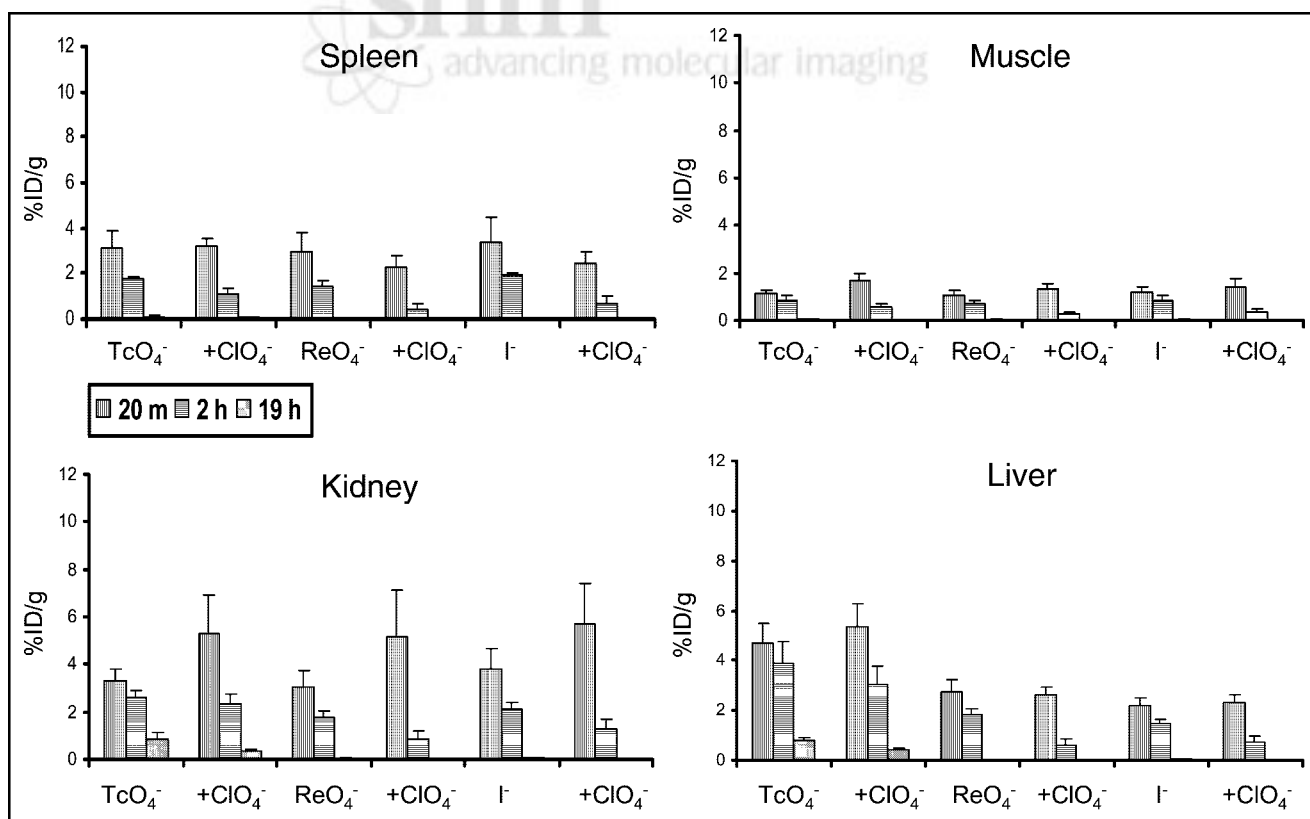


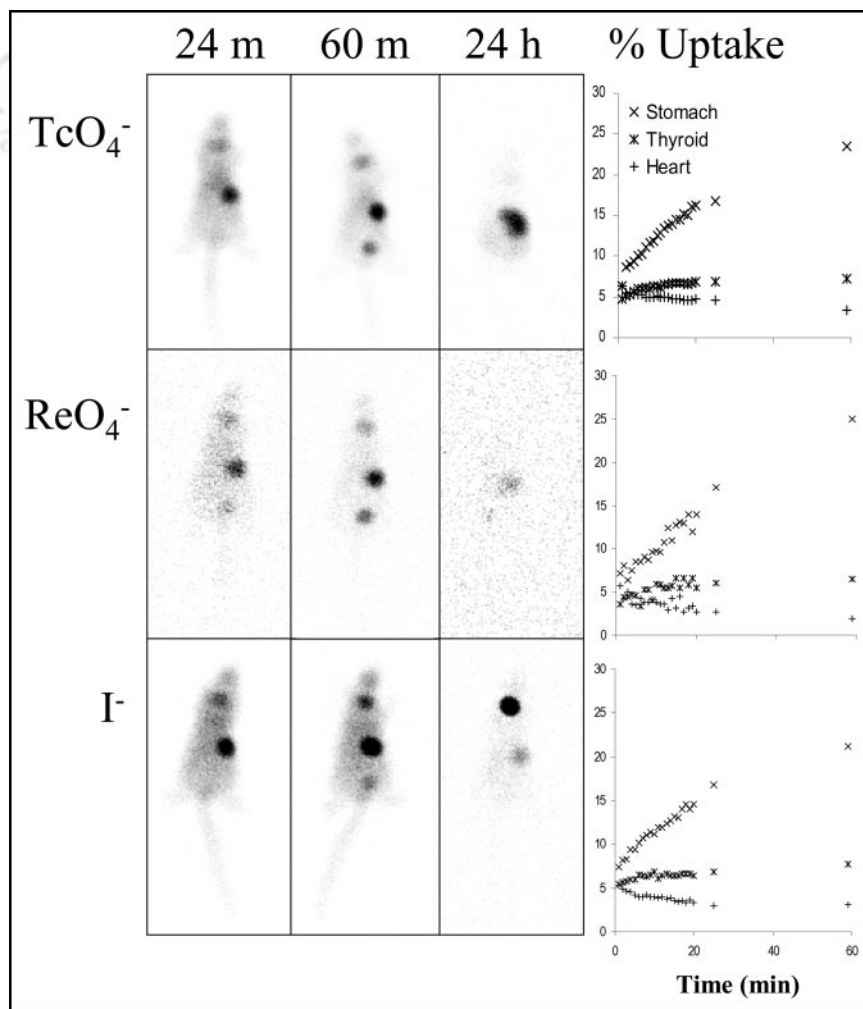
FIGURE 2. Activity in tissues that did not significantly express NIS (liver, muscle, spleen, kidney). Error bars represent 1 SD. The y-axis scale is similar to that of blood (Fig. 1). The 3 radiopharmaceuticals showed similar patterns of uptake. Activities were lower than those of blood and sequentially decreased over time. Addition of perchlorate did not diminish activity and, in fact, resulted in a modest increase in renal activity at 20 min, probably the result of a reduction in uptake by competing NIS-dependent pathways.

TABLE 1
Ratio of Injected Dose per Gram in Tissue to That in Blood

Time	Organ	Injected compound					
		Iodide	Iodide + ClO ₄ ⁻	TcO ₄ ⁻	TcO ₄ ⁻ + ClO ₄ ⁻	ReO ₄ ⁻	ReO ₄ ⁻ + ClO ₄ ⁻
20 min	Stomach	4.98 ± 2.09	0.31 ± 0.09	5.35 ± 2.15	0.22 ± 0.04	4.74 ± 2.16	0.19 ± 0.05
	Salivary gland	2.70 ± 0.89	0.41 ± 0.02	2.91 ± 1.08	0.30 ± 0.01	3.21 ± 0.97	0.31 ± 0.02
	Thyroid	3.02 ± 0.68	0.40 ± 0.03	1.87 ± 0.40	0.30 ± 0.04	2.04 ± 0.50	0.30 ± 0.04
	Liver	0.41 ± 0.03	0.38 ± 0.06	0.64 ± 0.07	0.57 ± 0.09	0.44 ± 0.03	0.34 ± 0.03
	Muscle	0.23 ± 0.02	0.23 ± 0.02	0.16 ± 0.02	0.18 ± 0.01	0.17 ± 0.02	0.17 ± 0.03
	Kidney	0.71 ± 0.15	0.92 ± 0.19	0.46 ± 0.02	0.56 ± 0.12	0.49 ± 0.03	0.67 ± 0.23
	Spleen	0.61 ± 0.11	0.39 ± 0.03	0.43 ± 0.05	0.34 ± 0.04	0.46 ± 0.09	0.29 ± 0.05
2 h	Stomach	10.87 ± 3.77	0.80 ± 0.33	15.04 ± 4.50	0.58 ± 0.28	11.86 ± 4.91	0.54 ± 0.20
	Salivary gland	3.90 ± 1.14	0.38 ± 0.13	4.40 ± 1.07	0.29 ± 0.10	4.91 ± 1.46	0.28 ± 0.09
	Thyroid	19.45 ± 5.95	0.44 ± 0.16	4.76 ± 0.35	0.28 ± 0.10	6.30 ± 1.05	0.29 ± 0.10
	Liver	0.41 ± 0.05	0.41 ± 0.17	0.88 ± 0.19	0.83 ± 0.30	0.50 ± 0.09	0.33 ± 0.10
	Muscle	0.25 ± 0.05	0.22 ± 0.09	0.19 ± 0.03	0.17 ± 0.07	0.18 ± 0.03	0.15 ± 0.04
	Kidney	0.59 ± 0.03	0.73 ± 0.39	0.59 ± 0.04	0.63 ± 0.19	0.48 ± 0.05	0.45 ± 0.11
	Spleen	0.54 ± 0.06	0.35 ± 0.11	0.39 ± 0.03	0.28 ± 0.09	0.38 ± 0.06	0.25 ± 0.09

Data are mean ± 1 SD. Because of negligible blood activity, stochastic noise precluded meaningful ratios at the 19-h time point.

FIGURE 3. Images in representative mice demonstrated the marked amount of gastric uptake noted for all 3 radiopharmaceuticals on the 24- and 60-min images. By 24 h, the activity was less well defined and, at least in the case of ^{99m}TcO₄⁻, more diffusely distributed within the bowel. For ^{99m}TcO₄⁻ and ¹⁸⁸ReO₄⁻, a modest amount of concentration of activity was seen in the region of the thyroid gland at 24 and 60 min, but this faded by the 24-h time point. In contrast, ¹²³I⁻ gradually increased between the 24-min, 60-min, and 24-h images. Rhenium-based curves exhibited increased noise as a result of the lower abundance of γ -photons for this radionuclide. Time-activity curves based on ROIs over the stomach, mediastinum, and thyroid demonstrated similar appearances for the 3 radiopharmaceuticals. Because of limitations in external photon scanning, apparent magnitude of uptake may be less than that based on actual organ counting. Uptake in the stomach was most intense and increased over the 1 h of initial imaging, concentrating 20%–25% of injected activity. Thyroid uptake was more modest and also increased over time (5%–7% of injected activity). Mediastinal activity, representing blood pool, gradually decreased over the initial 1 h of measurements, representing approximately 2% of injected activity at the 60-min time point.



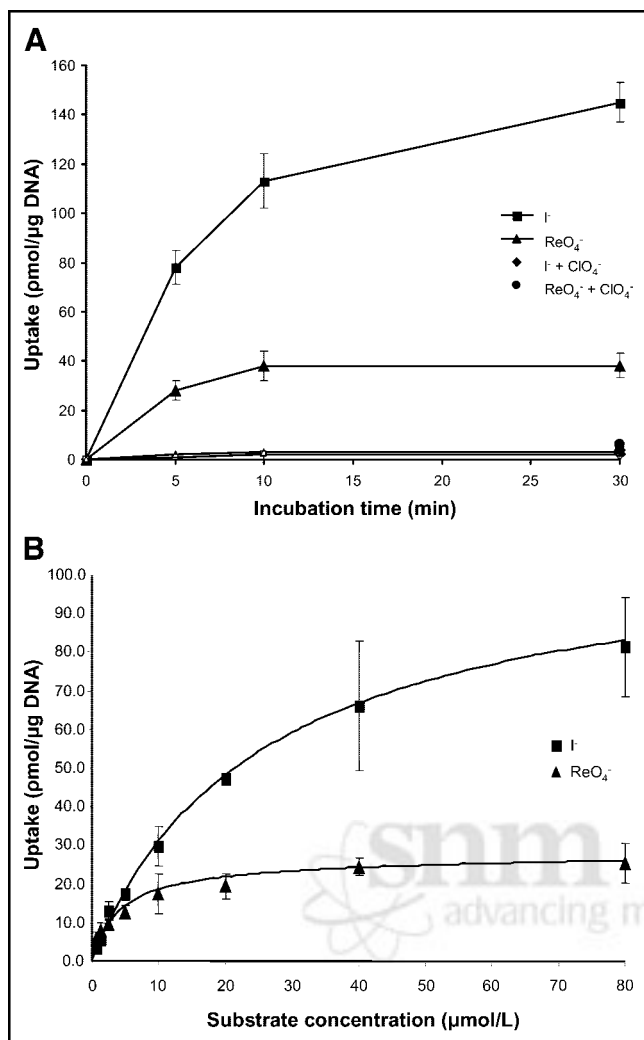


FIGURE 4. Uptake of iodide and perrhenate in hNIS-transfected MDCK cells. Error bars denote 1 SD. (A) Time course of uptake. Cells were incubated with 20 $\mu\text{mol/L}$ iodide or perrhenate supplemented with carrier-free $^{125}\text{I}^-$ and $^{188}\text{ReO}_4^-$, respectively, for the indicated periods of time. Solid symbols represent uptake in NIS-transfected cells, and open symbols represent uptake in nontransfected cells. Uptake of iodide exceeds that of perrhenate at all time points in the transfected cells. Transfected cells in the presence of the potent NIS inhibitor perchlorate and non-NIS-transfected MDCK cells did not concentrate either anion. (B) Kinetic analysis of iodide and perrhenate uptake into hNIS-transfected MDCK cells based on 2-min uptake values at variable substrate concentrations. V_{max} and K_m values were estimated using the Marquard–Levenberg algorithm as 106 ± 3.2 and 24.6 ± 1.81 pmol/ μg for iodide and 25.6 ± 1.4 and 4.06 ± 0.87 $\mu\text{mol/L}$ for perrhenate (plotted symbols represent experimental data and solid lines the fitted curves).

To determine the kinetic parameters of perrhenate uptake, initial uptake rates (2-min time points) were measured at different substrate concentrations. Saturation kinetics were observed (Fig. 4B). Based on the Marquard–Levenberg algorithm (28), the apparent V_{max} values for perrhenate and iodide were 25.6 ± 1.4 and 106 ± 3.2 pmol/ μg , respec-

tively, and the corresponding K_m values were 4.06 ± 0.87 and 24.6 ± 1.81 $\mu\text{mol/L}$.

DISCUSSION

Imaging and ROI analysis have graphically demonstrated the similarity of perrhenate distribution to distribution of pertechnetate and iodide. Because the administered concentrations of these substrates are so much lower than their K_m values, they are not believed to interfere with each other, assuming Michaelis–Menten kinetics.

When coadministered, pertechnetate, perrhenate, and iodide had similar uptake and biodistribution in NIS-expressing and non-NIS-expressing tissues, with the exception of the thyroid gland, where iodide continued to be retained through 19 h, as a result of organification. Activity in the NIS-bearing tissues exceeded the blood concentration of activity severalfold. Uptake was highest in the stomach, intermediate in the salivary gland, and lowest in the thyroid. Although this may reflect differential activity of the symporter in the various tissues, stomach activity may be artifactually increased as a result of retention of secreted activity within the lumen. Uptake values in the thyroid may also be artifactually decreased as a result of the unavoidable inclusion of nonthyroidal tissue in the samples, thereby diluting the per-gram uptake values. Perchlorate markedly abolished uptake by NIS-containing tissues while paradoxically increasing concentration in non-NIS-bearing tissues, presumably because of a lack of competitive uptake by the NIS-containing tissues. This phenomenon was also apparent in a previous study of rats, measured at 30 min after injection (22).

Our *in vivo* murine studies were supplemented with cell culture measurements in which the amount of substrate could be rigorously controlled. In cultured cells that permanently express NIS, perrhenate was transported with an affinity even greater than that of iodide, agreeing with previous measurements performed using other techniques (30). The higher affinities of perrhenate ($K_m = 4.06$ $\mu\text{mol/L}$) and iodide ($K_m = 24.6$ $\mu\text{mol/L}$) compared with those previously reported for ClO_3^- ($K_m = 277$ $\mu\text{mol/L}$) and NO_3^- ($K_m = 739$ $\mu\text{mol/L}$) may relate to their significantly larger ionic radii (1.88 Å for perrhenate, 2.2 Å for iodide, 1.66 Å for ClO_3^- , and 1.45 Å for NO_3^-), presumably leading to an improved symporter-binding fit (9,30,31).

In contrast to the present findings, in an earlier study using rat thyroid NIS expressed in *Xenopus laevis* oocytes, Eskandari et al. (9) did not detect perrhenate transport into the oocytes, although they found perrhenate to be a potent blocking agent for NIS, second only to perchlorate. It is possible that the lack of uptake reported on the basis of Eskandari's electrophysiologic measurements was the result of a 1:1 Na^+ /perrhenate stoichiometry or differences related to expression in amphibian

versus mammalian cells (32). The present results are less prone to artifacts in that we have used a stably transfected MDCK cell line to study uptake. NIS-dependent perhenate transport in MDCK cells is also corroborated by our whole-animal uptake studies of $^{188}\text{ReO}_4^-$, which demonstrated a high degree of uptake in NIS-containing tissues, qualitatively similar to that of $^{99\text{m}}\text{TcO}_4^-$ and $^{125}\text{I}^-$. Our data are qualitatively consistent with those recently reported by Van Sande et al. (33) in FRTL-5 cells and in NIS-transfected COS cells, although quantitatively different because we observed a 3- to 4-fold-higher accumulation of iodide as compared with perhenate (Figs. 4A and 4B), whereas Van Sande et al. reported a higher relative uptake for perhenate than iodide.

Because effective therapy depends on retention of radionuclide in the target, a major variable in the use of NIS-targeted therapy is the rate of egress of radionuclide from the tissue (34). Retention of iodide has been studied in tumors transfected with NIS, where short effective half-times of residence have been found (35–40). In an attempt to prolong the retention time of radioiodine in various tumor types, thyroperoxidase has been cotransfected in addition to NIS, with variable results (38,39). An alternative approach may be to optimize the characteristics of the therapeutic radionuclide (40). $^{188}\text{ReO}_4^-$ is a promising candidate based on its high uptake by NIS-expressing tissues and the energetic β^- emissions of ^{188}Re . The degree of uptake and retention may be sufficient for delivery of therapeutic doses of radiation to NIS-expressing tumors, considering the average β^- energy of ^{188}Re (which is almost 7-fold higher than that of $^{131}\text{I}^-$) and its considerably shorter physical half-life (17 h vs. 8 d for ^{131}I). In an experimental model of breast carcinoma, we have previously demonstrated that $^{188}\text{ReO}_4^-$ was able to deliver a dose to the tumor 4.5-fold higher per megabecquerel administered than $^{131}\text{I-NaI}$ (20). In fact, absent organification of perhenate by the thyroid gland may also be considered an advantage in therapy of nonthyroidal NIS-bearing tissues, in that the thyroid will not serve as a sink for radiopharmaceutical and will sustain less radiation damage. The currently available procedure to decrease uptake by the thyroid gland is the administration of exogenous thyroid hormone, which transiently down-regulates thyroid-NIS and thereby decreases radioiodine uptake.

CONCLUSION

As we enter into the era of NIS-based diagnostics and therapeutics, understanding the biologic behavior of perhenate in addition to that of iodide and pertechnetate will facilitate modeling and allow a rational choice of radionuclides with the most appropriate physical characteristics for imaging and therapy of NIS-expressing tumors.

ACKNOWLEDGMENTS

The authors acknowledge Dr. Judah Weinberger's assistance in obtaining perhenate. This work was supported in part by the National Institutes of Health DK-41544 (NC) and CA-95377 (ED).

REFERENCES

- Dai G, Levy O, Carrasco N. Cloning and characterization of the thyroid iodide transporter. *Nature*. 1996;379:458–460.
- Smanik PA, Liu Q, Furminger TL, et al. Cloning of the human sodium iodide symporter. *Biochem Biophys Res Commun*. 1996;226:339–345.
- Dohan O, De la Vieja A, Carrasco N. Molecular study of the sodium-iodide symporter (NIS): a new field in thyroidology. *Trends Endocrinol Metab*. 2000;11:99–105.
- De la Vieja A, Dohan O, Levy O, Carrasco N. Molecular analysis of the sodium/iodide symporter: impact on thyroid and extrathyroid pathophysiology. *Physiol Rev*. 2000;80:1083–1105.
- Riedel C, Dohan O, De la Vieja A, Ginter CS, Carrasco N. Journey of the iodide transporter NIS: from its molecular identification to its clinical role in cancer. *Trends Biochem Sci*. 2001;26:490–496.
- Shen DHY, Kloos RT, Mazzaferri EL, Jhian SM. Sodium iodide symporter in health and disease. *Thyroid*. 2001;11:415–425.
- Dohan O, Gavrielides MV, Ginter C, Amzel LM, Carrasco N. Na(+)/I(-) symporter activity requires a small and uncharged amino acid residue at position 395. *Mol Endocrinol*. 2002;16:1893–1902.
- Dohan O, De la Vieja A, Paroder V, et al. The sodium/iodide symporter (NIS): characterization, regulation, and medical significance. *Endocr Rev*. 2003;24:48–77.
- Eskandari S, Loo DD, Dai G, Levy O, Wright EM, Carrasco N. Thyroid Na+/I- symporter: mechanism, stoichiometry, and specificity. *J Biol Chem*. 1997;272:27230–27238.
- Wapnir IL, van de Rijn M, Nowels K, et al. Immunohistochemical profile of the sodium/iodide symporter in thyroid, breast, and other carcinomas using high density tissue microarrays and conventional sections. *J Clin Endocrinol Metab*. 2003;88:1880–1888.
- Tazebay UH, Wapnir IL, Levy O, et al. The mammary gland iodide transporter is expressed during lactation and in breast cancer. *Nat Med*. 2000;6:871–878.
- Kilbane MT, Ajjan RA, Weetman AP, et al. Tissue iodine content and serum-mediated ^{125}I uptake-blocking activity in breast cancer. *J Clin Endocrinol Metab*. 2000;85:1245–1250.
- Boland A, Ricard M, Opolon P, et al. Adenovirus-mediated transfer of the thyroid sodium/iodide symporter gene into tumors for a targeted radiotherapy. *Cancer Res*. 2000;60:3484–3492.
- Mandell RB, Mandell LZ, Link CJ Jr. Radioisotope concentrator gene therapy using the sodium/iodide symporter gene. *Cancer Res*. 1999;59:661–668.
- Nakamoto Y, Saga T, Misaki T, et al. Establishment and characterization of a breast cancer cell line expressing Na+/I- symporters for radioiodide concentrator gene therapy. *J Nucl Med*. 2000;41:1898–1904.
- Spitzweg C, Harrington KJ, Pinke LA, Vile RG, Morris JC. Clinical review 132: the sodium iodide symporter and its potential role in cancer therapy. *J Clin Endocrinol Metab*. 2001;86:3327–3335.
- Emamian SA, Shalaby-Rana E, Majd M. The spectrum of heterotopic gastric mucosa in children detected by Tc-99m pertechnetate scintigraphy. *Clin Nucl Med*. 2001;26:529–535.
- Berquist TH, Nolan NG, Stephens DH, Carlson HC. Specificity of $^{99\text{m}}\text{Tc}$ -pertechnetate in scintigraphic diagnosis of Meckel's diverticulum: review of 100 cases. *J Nucl Med*. 1976;17:465–469.
- Meine FJ, Woloshin HJ. Radiologic diagnosis of salivary gland tumors. *Radiol Clin North Am*. 1970;8:475–485.
- Dadachova E, Bouzahzah B, Zuckier LS, Pestell RG. Rhenium-188 as an alternative to iodine-131 for treatment of breast tumors expressing the sodium/iodide symporter (NIS). *Nucl Med Biol*. 2002;29:13–18.
- Saha GP. *Fundamentals of Nuclear Pharmacy*. New York, NY: Springer-Verlag; 1997.
- Lin WY, Hsieh JF, Tsai SC, Yen TC, Wang SJ, Knapp FF Jr. A comprehensive study on the blockage of thyroid and gastric uptakes of ^{188}Re -perhenate in endovascular irradiation using liquid-filled balloon to prevent restenosis. *Nucl Med Biol*. 2000;27:83–87.
- Lin WY, Tsai SC, Hsieh BT, Lee TW, Ting G, Wang SJ. Evaluation of three

- rhenum-188 candidates for intravascular radiation therapy with liquid-filled balloons to prevent restenosis. *J Nucl Cardiol*. 2000;7:37–42.
24. Deutsch E, Libson K, Vanderheyden JL, Ketring AR, Maxon HR. The chemistry of rhenium and technetium as related to the use of isotopes of these elements in therapeutic and diagnostic nuclear medicine. *Int J Rad Appl Instrum B*. 1986;13:465–477.
 25. Groot-Wassink T, Aboagye EO, Glaser M, Lemoine NR, Vassaux G. Adenovirus biodistribution and noninvasive imaging of gene expression in vivo by positron emission tomography using human sodium/iodide symporter as reporter gene. *Hum Gene Ther*. 2002;13:1723–1735.
 26. Weiss SJ, Philp NJ, Grollman EF. Iodide transport in a continuous line of cultured cells from rat thyroid. *Endocrinology*. 1984;114:1090–1098.
 27. Levy O, Dai G, Riedel C, et al. Characterization of the thyroid Na⁺/I⁻ symporter with an anti-COOH terminus antibody. *Proc Natl Acad Sci USA*. 1997;94:5568–5573.
 28. Press WH, Flannery BP, Teukolsky SA, Wetterling WT. *Numerical Recipes: The Art of Scientific Computing*. Cambridge, UK: Cambridge University Press; 1986.
 29. Spitzweg C, Dutton CM, Castro MR, et al. Expression of the sodium iodide symporter in human kidney. *Kidney Int*. 2001;59:1013–1023.
 30. Wolff J. Transport of iodide and other anions in the thyroid gland. *Physiol Rev*. 1964;44:45–90.
 31. Halmi NS. Thyroidal iodide transport. *Vitam Horm*. 1961;19:133–163.
 32. Wolff J. Perchlorate and the thyroid gland. *Pharmacol Rev*. 1998;50:89–105.
 33. Van Sande J, Massart C, Beauwens R, et al. Anion selectivity by the sodium iodide symporter. *Endocrinology*. 2003;144:247–252.
 34. Cho JY, Xing S, Liu X, et al. Expression and activity of human Na⁺/I⁻ symporter in human glioma cells by adenovirus-mediated gene delivery. *Gene Ther*. 2000;7:740–749.
 35. Shimura H, Haraguchi K, Miyazaki A, Endo T, Onaya T. Iodide uptake and experimental ¹³¹I therapy in transplanted undifferentiated thyroid cancer cells expressing the Na⁺/I⁻ symporter gene. *Endocrinology*. 1997;138:4493–4496.
 36. Smit JW, Shroder-van der Elst JP, Karperien M, et al. Reestablishment of in vitro and in vivo iodide uptake by transfection of the human sodium iodide symporter (hNIS) in a hNIS defective human thyroid carcinoma cell line. *Thyroid*. 2000;10:939–943.
 37. Haberkorn U, Henze M, Altmann A, et al. Transfer of the human NaI symporter gene enhances iodide uptake in hepatoma cells. *J Nucl Med*. 2001;42:317–325.
 38. Huang M, Batra RK, Kogai T, et al. Ectopic expression of the thyroperoxidase gene augments radioiodide uptake and retention mediated by the sodium iodide symporter in non-small cell lung cancer. *Cancer Gene Ther*. 2001;8:612–618.
 39. Boland A, Magnon C, Filetti S, et al. Transposition of the thyroid iodide uptake and organification system in nonthyroid tumor cells by adenoviral vector-mediated gene transfers. *Thyroid*. 2002;12:19–26.
 40. Haberkorn U, Kinscherf R, Kissel M, et al. Enhanced iodide transport after transfer of the human sodium iodide symporter gene is associated with lack of retention and low absorbed dose. *Gene Ther*. 2003;10:774–780.

